

Paper

Harbingers and latecomers - The order of appearance of exact coherent structures in plane Poiseuille flow

Stefan Zammert^{a*} and Bruno Eckhardt^b^a*Fachbereich Physik, Philipps-Universität Marburg,
Renthof 6, D-35032 Marburg, Germany;*^b*J.M. Burgerscentrum, Delft University of Technology,
2628 CD Delft, The Netherlands**(Received 00 Month 200x; final version received 00 Month 200x)*

The transition to turbulence in plane Poiseuille flow (PPF) is connected with the presence of exact coherent structures. In contrast to other shear flows, PPF has a number of different coherent states that are relevant for the transition. We here discuss the different states, compare the critical Reynolds numbers and optimal wavelengths for their appearance, and explore the differences between flows operating at constant mass flux or at constant pressure drop. The Reynolds numbers quoted here are based on the mean flow velocity and refer to constant mass flux, the ones for constant pressure drop are always higher. The Tollmien-Schlichting waves bifurcate subcritically from the laminar profile at $Re = 5772$ and reach down to $Re = 2609$ (at a different optimal wave length). Their localized counter part bifurcates at the even lower value $Re = 2334$. Three dimensional exact solutions appear at much lower Reynolds numbers. We describe one exact solutions that is spanwise localized and has a critical Reynolds number of 316. Comparison to plane Couette flow suggests that this is likely the lowest Reynolds number for exact coherent structures in PPF. Streamwise localized versions of this state require higher Reynolds numbers, with the lowest bifurcation occurring near $Re = 1018$.

Keywords: Transition; Chaos and Fractals; Vortex Dynamics

1. Introduction

Within the last decade many fully 3d exact coherent states of the Navier-Stokes equations have been identified. They are important for understanding the transition to turbulence in various shear flows, for determining the thresholds for the transition, and for characterizing the subsequent evolution towards fully developed turbulence [1, 2]. Coherent structures provide a scaffold for the turbulent time evolution because they are embedded in the turbulent dynamics [3] and form a network of heteroclinic connections [4]. Tracking exact coherent states also provided insights into the formation of the chaotic saddles and transient turbulence in plane Couette, pipe, and plane Poiseuille flow (PPF) [5–7]. Special coherent structures, so called edge states [8], are important for the transition to turbulence since their stable manifold separates the state space in a part with turbulence and another one where initial conditions relaminarize directly.

Among the various shear flows that have been studied, PPF is special because it also has a linear instability of the laminar profile which triggers Tollmien-Schlichting (TS) waves [9]. The extend to which they contribute to the observed

*Corresponding author. Email: Stefan.Zammert@physik.uni-marburg.de

transition then depends on the order of appearance of the different states. As we will see, some states are *harbingers* that appear well below the experimentally observed transition, and others are *latecommers*, appearing well above the transition. Harbingers prepare the experimentally observed transition to turbulent dynamics, and latecomers add additional states and degrees of freedom at higher Reynolds numbers.

While critical Reynolds numbers for linear instabilities of the laminar profile are well defined and unique, this is not the case for the subcritical transitions to be discussed here. For the subcritical case, it does make a difference whether the system is run under conditions of constant mass flux or prescribed pressure or perhaps constant energy input [10]. All exact coherent states have a fixed relation between pressure drop and mean flow rate, but the quest for the bifurcation point focusses on different projections and hence gives different critical Reynolds numbers depending on whether the flow rate or the pressure drop or some other quantity are kept constant.

The setting of operating conditions also affects the choice of Reynolds numbers. To be specific, we define

$$Re_B = \frac{3U_B d}{2\nu}, \quad (1)$$

for the case of constant mean bulk velocity U_B . The other parameters are d , half the channel width and ν , the kinematic viscosity. If the pressure gradient is fixed, we define the pressure based Reynolds number,

$$Re_P = \frac{U_{cl,P} d}{\nu}, \quad (2)$$

where $U_{cl,P} = d^2(dP/dx)/2\nu$ is the laminar centerline velocity for this value of the pressure gradient. The numerical factors in (1) are chosen such that the two Reynolds numbers agree for the case of a laminar profile, $Re_B = Re_P$. For 3d coherent states they are usually different. Therefore, even if the laminar state coincides, the state space of the system at different operating conditions may be different, because in one case some exact coherent structure might already exist that are not yet present in the other case.

For direct numerical simulation we used *Channelflow*-code (www.channelflow.org) [11]. Exact coherent structures were identified and continued in Reynolds number using the Newton hookstep [see e.g. 12] continuation methods [see e.g. 13] included in the *Channelflow*-package.

2. Spatially extended and localized Tollmien-Schlichting waves

The laminar state of PPF has a subcritical instability. The exact values for the critical Reynolds number and wavelength have remained unclear [14–16] until the issue was finally settled by Orszag [17], who calculated a critical Reynolds number of 5772.22 for a critical wavelength of 1.96π using spectral methods. Chen & Joseph [18] then demonstrated the existence of two-dimensional travelling wave solutions, so-called finite amplitude TS-waves, bifurcating subcritically from the laminar flow. These two-dimensional exact coherent structures were later studied by Zahn et al. [19], Jimenez [20] and Soibelman & Meiron [21]. Estimates for the lowest Reynolds number of the turning points were first given by Grohne [22] and Zahn et al. [19]. Using a truncation after one or two modes they found that the traveling waves

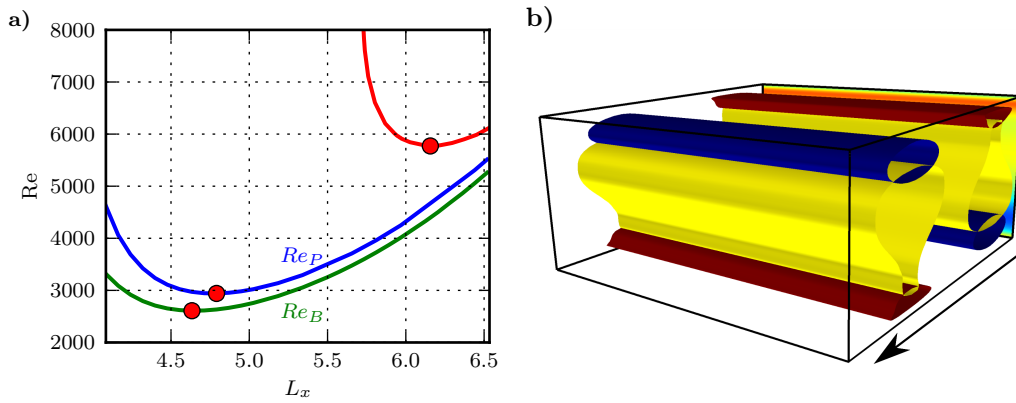


Figure 1. Tollmien-Schlichting waves in PPF. (a) Instability of the laminar profile (red) and existence regions for spatially extended TS waves. The green and blue lines show the Reynolds number of the turning point vs. streamwise wavelength L_x for the constant mean flow (green) and constant pressure gradient (blue), respectively. The minima of the curves are marked by a red circle: $Re = 5772$ and $\lambda = 6.16$ for the linear instability of the laminar profile, $Re_B = 2609$ and $\lambda = 4.65$ for constant mass flux and $Re_P = 2941$ and $\lambda = 4.81$ for constant pressure drop. (b) Visualization of the TS wave for the minimal Reynolds number at constant mass flux. The direction of the flow is indicated by the black arrow. An iso-surface 0.01 of the Q-vortex criterion is shown in yellow. Iso-surfaces ± 0.12 of the streamwise velocity (deviation from laminar) are shown in blue and red.

appear slightly above $Re = 2700$. Their result were qualitatively confirmed in later studies using a higher number of modes [23].

In our numerical simulations we use the *channelflow*-code with resolution $N_x \times N_y \times N_z = 80 \times 97 \times 4$. The streamwise and spanwise resolution is chosen sufficiently fine to ensure that a further increase does not change the obtained Reynolds numbers. The code is set up to solve the fully 3d problem, however, it can be reduced to an effectively 2d code with the choice of $N_z = 4$, since all the modes with $k_z \neq 0$ enter with zero amplitude. We therefore can stay within the same algorithmic framework and code and can exploit all the modules of *channelflow*.

We identify the traveling waves that bifurcate from the laminar flow (referred to as TW_{TS} in the following) using a Newton-method and continue them in Reynolds number with the continuation methods within *channelflow*. Figure 1a) shows the bifurcation diagram versus streamwise wavelength. The stability curve for the laminar profile is the same for the constant pressure gradient and constant mass flux case, and has a minimum at $Re = 5772$ and a wavelength of 6.16. The bifurcation is subcritical and reaches to lower Reynolds numbers, but these points then depend on the operating conditions: the minimal values are $Re_B = 2609$ and $Re_P = 2941$. The critical wavelengths are 4.65 and 4.81, respectively, and thus smaller than the one for the linear instability of the laminar profile.

The flow field of TW_{TS} at the the minimal Reynolds number $Re_B = 2609$ is visualized in figure 1b).

In a study on two-dimensional PPF, Jimenez [20] discovered streamwise modulated packages of TS-waves. They have a turning point significantly lower than the spatially extended traveling wave TW_{TS} [24]. In even longer domains, they turn into fully localized states that are relative periodic orbits, generated out of subharmonic instabilities of the spatially extended TS waves [25, 26]. Figure 2a) shows a bifurcation diagram for the modulated TS-waves and the spatially extended traveling wave from which they bifurcate. The ordinate of the diagram is the amplitude of the flow field,

$$a(\mathbf{u}) = \sqrt{\frac{1}{2L_x L_z} \int \mathbf{u}^2 dx dy dz}, \quad (3)$$

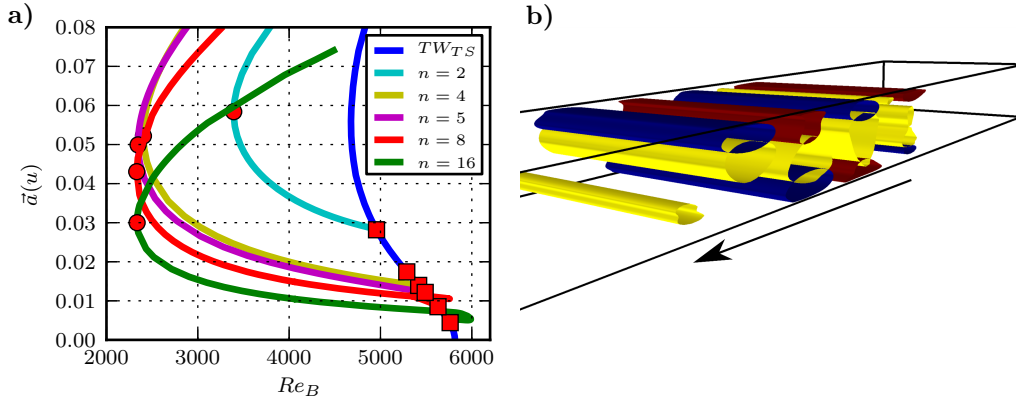


Figure 2. Localized TS-waves. (a) Bifurcations off the extended state for different domain widths. The black line shows the spatial extended TS-wave with streamwise wavelength $\lambda_0 = 2\pi$ and the colored lines show bifurcating periodic orbits corresponding to streamwise wavelengths $n\lambda_0$, where n is integer 2 and 16. The squares indicate the bifurcations of the extended state, and the circles the minimal critical Reynolds numbers for the different domains, from which a global minimum of $Re_B = 2335$ is estimated. (b) Localized TS-wave with $L_x = 16\lambda_0$ at the minimum $Re_B = 2335$. Isosurfaces of $Q = 0.01$ are shown in yellow, isosurfaces of $u = 0.1$ and $u = -0.1$ in red and blue.

where L_x and L_z are the streamwise and spanwise wavelengths of the computational domain. The spatially extended TS-wave shown in the figure has a wavelength $\lambda_0 = 2\pi$ and the localized and modulated TS-waves are created in Hopf-bifurcations that correspond to streamwise wavelengths L_x between 4 to 16 times λ_0 . Just above their bifurcations all solutions are modulated TS-waves but if the wavelength of the modulation is sufficiently long they become increasingly more localized with decreasing Re_B . E.g. for the short modulation wavelength $\Lambda = 6\lambda_0$, the solution is modulated but extends across the domain, whereas for $L_x = 16\lambda_0$ it becomes well localized at low Reynolds numbers.

The lowest Reynolds numbers for the turning point are $Re_B = 2335$ and $Re_P = 2372$ and are achieved for the localized TS-wave with modulation wavelength $16\lambda_0$. Further increasing the modulation wavelength does not change the localized state and does not result in significant changes of the Reynolds number for the turning point.

The spatially extended states as well as their localized counter-parts are extremely unstable to three-dimensional disturbances. However, the lower branches are stable against super-harmonic two-dimensional disturbances. The superharmonic bifurcations of the spatially extended TS-waves were investigated in detail by Casas and Jorba [27], who found that the upper branch of TW_{TS} undergoes Hopf bifurcations creating periodic state for the case of constant pressure gradient as well as for constant mass flux.

The lower branch of the streamwise localized TS-wave has only one unstable eigenvalue in the two-dimensional subspace and thus it is the edge state of the system [5, 8]. The upper branches undergo further bifurcations, leading to a chaotic temporal evolution. For the localized TS-wave, the upper branch undergoes a Hopf bifurcation and adds another frequency at $Re_B = 4470$. Further bifurcations of this quasi-periodic state add additional frequencies leading to a chaotic state. In figure 3a) a bifurcation diagram that includes the localized TS-wave and the bifurcating states is given. The Hopf bifurcation of the upper branch is marked in the figure by a red square.

For $Re_B > 4493$ the chaotic state becomes unstable and spontaneous transitions to a spatially extended chaotic state are possible. An example of a trajectory which spends several thousand time units in the vicinity of the localized chaotic state before it switches to the spatially extended state is shown in figure 3b).

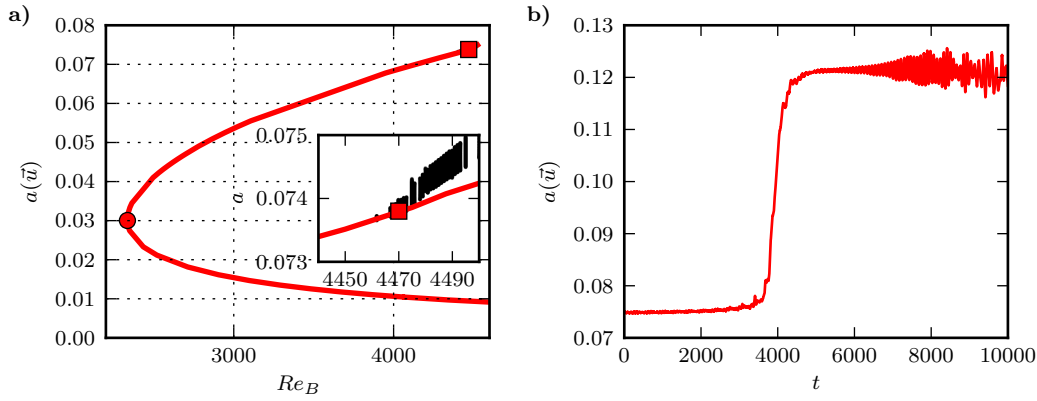


Figure 3. Bifurcations of localized TS-waves. (a) The upper branch of the localized TS-wave undergoes a Hopf bifurcation at $Re_B = 4470$ (red square) to a state with two frequencies. The states are indicated by the minima in a , which for a periodic orbit gives one point, and for the quasiperiodic one a line (see inset). The turning point is marked by a red dot, the bifurcation point by a red disk. (b) For even higher Reynolds numbers, the localized state undergoes a transition to a spatially extended state, here illustrated with the time trace of $a(t)$ for a state with $Re_B = 4496$. The sharp increase at times $O(4000)$ marks the transition from the localized to an extended state.

3. Three-dimensional travelling waves

The first three-dimensional solutions for PPF were described by Ehrenstein & Koch [28]. They found three-dimensional traveling waves below the saddle-node point of the two-dimensional TS-waves and studied their dependence on the streamwise and spanwise wavelength. However, their calculation were strongly truncated and attempts to reproduce their results with better resolution failed [29]. Subsequent studies identified many other three-dimensional exact solutions for PPF [29–34]. Waleffe [35] and Nagata & Deguchi [29] studied the dependence of particular solutions on the streamwise and spanwise wavelengths. They give as estimates for the lowest critical Reynolds numbers for the appearance of a traveling wave the values $Re_B = 615$ for $L_z = 1.55\pi$ and $L_x = 1.14\pi$ in the case of constant mass flux, and $Re_P = 805.5$ for $L_x = 1.504\pi$, $L_z = 1.156\pi$ in the case of constant pressure drop.

In this section, we investigate a special three-dimensional coherent structure, obtained by tracking the edge state [8, 36] in appropriately chosen computational domains. We use a numerical resolution of $N_x \times N_y \times N_z = 32 \times 65 \times 64$ for small domains and increase it to $N_x \times N_y \times N_z = 80 \times 65 \times 112$ for a domain with $L_x = L_z = 4\pi$. For sufficiently large domains the edge state of PPF is a traveling wave [33] that is symmetric with respect to the center-plane,

$$s_y : [u, v, w](x, y, z) = [u, -v, w](x, -y, z), \quad (4)$$

and obeys a shift-and reflect symmetry in addition,

$$s_z \tau_x(\lambda_x/2) : [u, v, w](x, y, z) = [u, v, -w](x + \lambda_x/2, y, -z). \quad (5)$$

To obtain the optimal wavelengths for this travelling wave, referred to as TW_E in the following, we studied the dependence of the critical Reynolds number on the streamwise and spanwise wavelength. In a straightforward scan of the wavelength domain with a stepping width of 0.1π and 0.05π in the spanwise and streamwise direction, respectively, we obtained the results shown in figure 4. The optimal Reynolds number is marked by a star.

As indicated by the white lines in figure 4, the lowest Reynolds numbers for the turning points are achieved if spanwise and streamwise wavelengths are of

comparable size for small wavelengths where the states are not localized in spanwise direction. In wide domains, for sufficiently large L_z , the solution becomes localized in the spanwise direction, and the turning point depends on L_x only. The lowest bulk Reynolds number for the turning point is 315.8 and achieved of $L_x = 2.9\pi$ and a width $L_z = 3.05\pi$. A visualization of the flow structures for these critical parameter values is given in figure 5. The lowest values of the pressure Reynolds number is $Re_P = 339.1$, which is also achieved for $L_x = 2.9\pi$ and $L_z = 3.05\pi$. Both minimal Reynolds numbers are much lower than those reported in previous studies [29, 35].

The optimal state TW_E may be compared to the coherent states in plane Couette flow. There, the lowest critical Reynolds number for the appearance of exact coherent structures is 127.705 [35, 37], based on half the channel height, and half the velocity difference between the plates. PPF is like two plane Couette flows staggered on top of each other, though with different boundary conditions (free slip instead of rigid) at the interface. For the Reynolds numbers one then has to take into account that the mean velocity in PPF corresponds to the full velocity difference between the plates in plane Couette flow, and half the channel width corresponds to the full gap. Therefore, when comparing Reynolds numbers, the ones from the usual definition of plane Couette flow have to be multiplied by four. Using this redefinition of the Reynolds number, the minimal Reynolds number of $Re = 127.705$ for plane Couette flow corresponds to $Re_B = 510$ for PPF. The proper steps for this comparison were done taken by Waleffe [35], who implemented a homotopy between the two flows, including the boundary conditions. He finds an optimal Reynolds number $Re_B \approx 642$. Moreover, the optimal wavelength for his state are $L_x = 1.86\pi$ and $L_z = 0.74$, much shorter and narrower than for the state described here (see figure 4). Therefore, for the time being, the travelling wave TW_E described here is the lowest lying critical state for plane Poiseuille flow.

For the combination of wavelengths giving the lowest values of Re_B for the turning point, the bifurcation diagram of TW_E is shown in figure 6. In a subspace with the symmetries s_y and $s_z\tau_x(\lambda_x/2)$ the the upper branch of TW_E is stable for $Re_B < 328.6$. At this Reynolds number the traveling wave undergoes a Hopf bifurcation, creating a periodic orbit which is stable in the symmetric subspace. In further bifurcation a chaotic attractor is created which remains stable in the subspace. The attractor is visualized in figure 6 by plotting minima and maxima of $a(\vec{u})$ for a trajectory on the attractor.

4. Streamwise localized three-dimensional periodic orbits

In spatially extended computational domains the edge state TW_E undergoes long-wavelength instabilities creating modulated and localized exact solutions [38]. In particular, a subcritical long-wavelength instability of TW_E at high Reynolds numbers creates a streamwise localized periodic orbit, henceforth referred to as PO_E , which is an edge state in long computational domains [33] and appears at low Reynolds numbers in a saddle-node bifurcation. The dependence of the Reynolds number of this saddle-node bifurcation on the spanwise wavelength is shown in figure 7a). The lowest Reynolds number for the turning point is achieved for a spanwise wavelength of 1.75π . For this value of L_z the bifurcation point lies at $Re_B = 1018.5$ and $Re_P = 1023.18$, respectively. For large values of L_z also the orbit PO_E becomes localized in spanwise direction [33], but for this spanwise wavelengths the bifurcation point lies at a much higher Reynolds number. A visualization of PO_E for the minimal bulk Reynolds number is shown in figure 7b).

While the localized TS waves, which also arise out of a subharmonic instability of

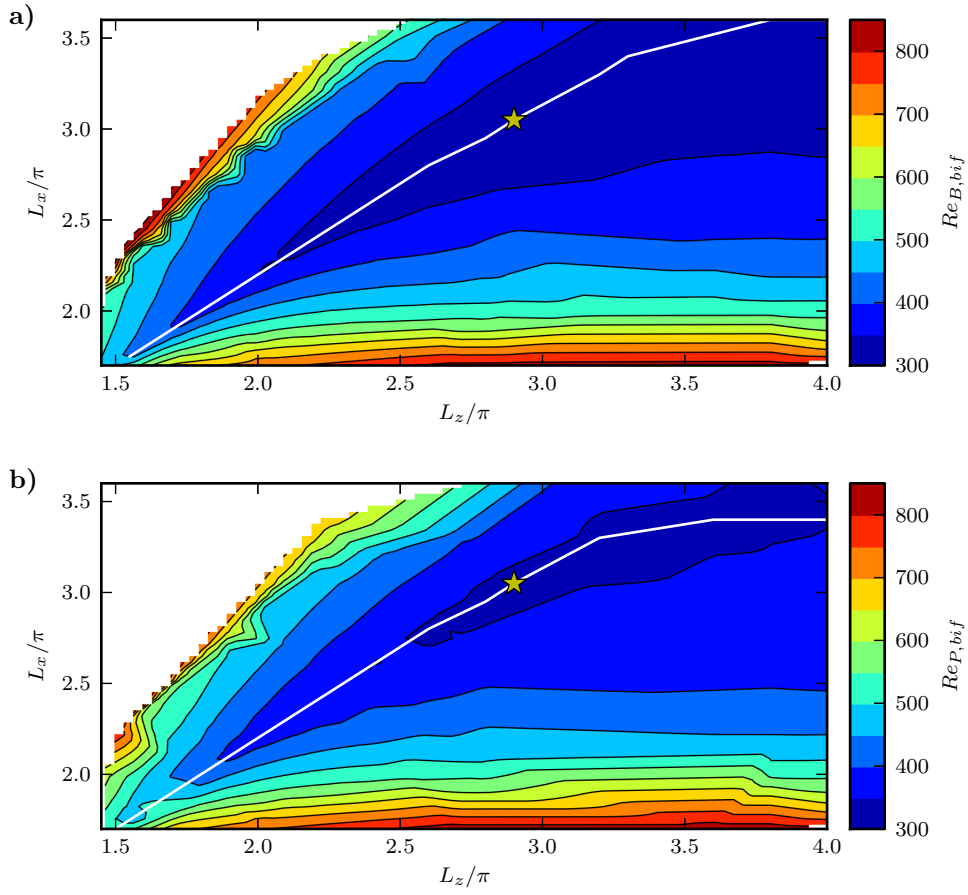


Figure 4. Wavelengths dependence of the critical Reynolds numbers for the traveling wave TW_E for (a) constant mean flow and (b) constant pressure drop. The Reynolds number is color coded and the optimal values are marked by a star. They are $Re_B = 315.8$ for constant mean flow, and $Re_P = 339.1$ at for constant pressure drop. In both cases the corresponding wavelength are $L_x = 2.9\pi$ and $L_z = 3.05\pi$. The white line marks the optimal L_x for a given L_z .

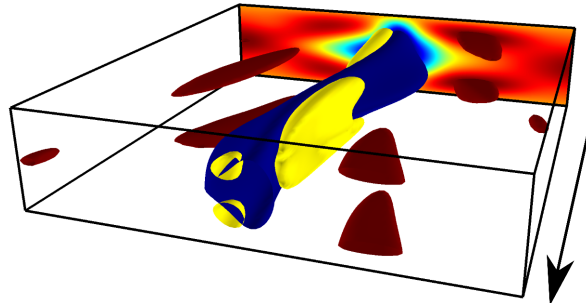


Figure 5. Instantaneous snapshot of TW_E for $L_x = 2.9\pi$ and $L_z = 3.05\pi$ at the turning point at $Re_B = 315.8$. Iso-surfaces of $Q = 0.01$ are shown in yellow, isosurfaces of $u = 0.1, -0.25$ of the streamwise velocity component (deviation from the laminar profile) in red and blue. The direction of the flow is indicated by the black arrow.

a spatially extended state, exist at lower Reynolds numbers than the corresponding spatially extended solutions, the localized orbit PO_E appears at much higher Reynolds number than its corresponding spatially extended solution TW_E .

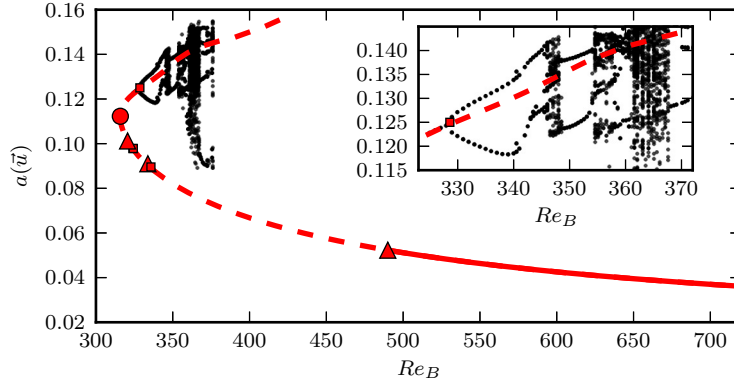


Figure 6. Bifurcation diagram of TW_E for the spatial wavelengths leading to the lowest bulk Reynolds number for the bifurcation point. For Reynolds numbers where the wave has only one unstable direction ($Re_B > 490$) a solid red line is used, while if the wave has more unstable directions a dashed line is used. The turning point is marked by a red dot. Red squares mark the positions of a Hopf bifurcations and triangles those of pitchfork bifurcations. The black dots are obtained from maxima and minima during the time-evolution. They indicate further bifurcations and the appearance of temporal chaos.

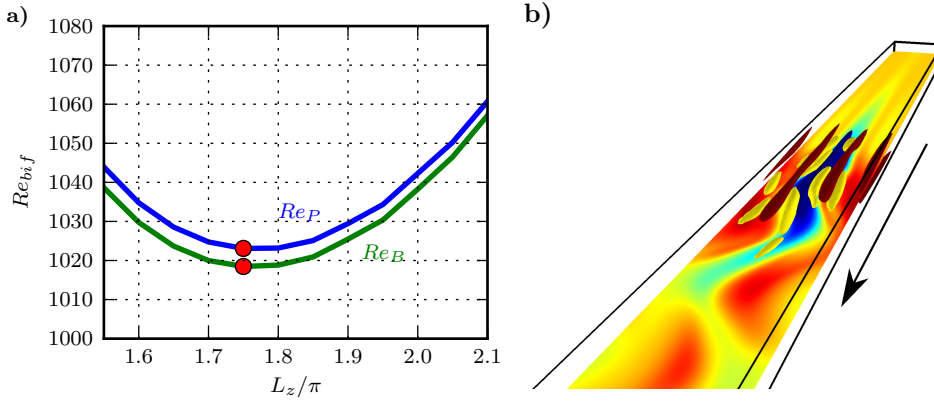


Figure 7. The localized periodic orbit PO_E . (a) Reynolds number of the bifurcation point of PO_E in dependence on the spanwise wavenumber L_z . Note that while the critical Reynolds numbers again vary between constant mean flow and constant pressure drop, but the optimal wavelengths coincide. (b) Instantaneous snapshot of PO_E for $L_z = 1.75\pi$ and $Re_B = Re_{B,min}(PO_E) = 1018.5$. Isosurfaces of $Q = 0.002$ are shown in yellow and isosurfaces $u = 0.075, -0.15$ of the streamwise velocity component (deviation from the laminar profile) in red and blue. The direction of the flow is indicated by the black arrow. In the center-plane the streamwise velocity is color-coded from blue to red.

5. Summary and conclusion

The different states and their critical Reynolds numbers and wavelengths are summarized in table 1. It is interesting to see that for the TS-waves, the localized structures appear before the extended ones, whereas for the 3d states the localized ones have a higher critical Reynolds number. Moreover, all TS waves appear well above the experimentally observed onset of turbulence, near $Re_B \approx 1000$ [9].

The traveling wave TW_E appears at very low Reynolds number, well below the experimentally observed onset of turbulence. The bifurcation diagram in figure 6 shows the usual increase in complexity and the presence of a crisis bifurcation, in which the attractor turns into a repeller and the dynamics becomes transient. In addition to the states discussed here, there are a variety of bifurcations in which spanwise localized and doubly-localized solution branch off from TW_E . All of these states, as well as exact coherent structures with different flow fields contribute to the temporal evolution, and the network that forms with increasing Reynolds numbers and that can then carry the turbulent dynamics.

Table 1. Critical values for the different bifurcations in PPF. The columns give the critical Reynolds numbers Re_B and Re_P and the associated optimal wavelengths for exact coherent structures and the laminar profile.

	$Re_{B,min}$	L_x	L_z	$Re_{P,min}$	$Re_{\tau,min}$	L_x	L_z
TW_{TS}	2610	1.48π	-	2941	76.7	1.53π	-
Localized TS	2334	-	-	2373	68.9	-	-
TW_E	315.8	3.05π	2.9π	339.1	26.04	3.05π	2.9π
PO_E	1018.5	-	1.75π	1023.18	45.23	-	1.75π
Laminar state	5772.22	1.96π	-	5722.22	196.98	1.96π	-

Very little is known about the lowest possible Reynolds number for the appearance of coherent structures, and there are hardly any methods for determining them reliably [39–41]. However, the state TW_E has the potential to be the lowest possible state in PPF flow by analogy to the lowest lying state in plane Couette flow. Identification of lower lying exact coherent structures in either flow should therefore also have implications for the other flow.

Among the exact coherent structures, TW_E is a harbinger for the occurrence of turbulence, whereas the two dimensional TS-wave are latecomers. They do not contribute to the formation of subcritical transition at low Reynolds, but are related to a secondary path to turbulence in PPF that can be realized if special precautions are taken to prevent the faster transition via 3d structures.

This work was supported in part by the DFG within FOR 1182.

References

- [1] B. Eckhardt, T.M. Schneider, B. Hof, and J. Westerweel, *Turbulence transition in pipe flow*, Annu Rev Fluid Mech 39 (2007), pp. 447–468.
- [2] B. Eckhardt, *Turbulence transition in pipe flow: some open questions*, Nonlinearity 21 (2008), pp. T1–T11.
- [3] G. Kawahara, and S. Kida, *Periodic motion embedded in plane Couette turbulence: regeneration cycle and burst*, J. Fluid Mech. 449 (2001), pp. 291–300.
- [4] J. Halcrow, J.F. Gibson, P. Cvitanović, and D. Viswanath, *Heteroclinic connections in plane Couette flow*, J. Fluid Mech. 621 (2009), p. 365.
- [5] T. Kreilos, and B. Eckhardt, *Periodic orbits near onset of chaos in plane Couette flow.*, Chaos 22 (2012), p. 047505.
- [6] M. Avila, F. Mellibovsky, N. Roland, and B. Hof, *Streamwise-Localized Solutions at the Onset of Turbulence in Pipe Flow*, Phys. Rev. Lett. 110 (2013), p. 224502.
- [7] S. Zammert, and B. Eckhardt, *Crisis bifurcations in plane Poiseuille flow*, Phys. Rev. E 91 (2015), p. 041003(R).
- [8] J. Skufca, J.A. Yorke, and B. Eckhardt, *Edge of Chaos in a Parallel Shear Flow*, Phys. Rev. Lett. 96 (2006), p. 174101.
- [9] P. Schmid, and D.S. Henningson *Stability and transition in shear flow*, Springer Berlin / Heidelberg, 2001.
- [10] H. Yosuke, M. Quadrio, and B. Frohnappfel, *Numerical simulation of turbulent duct flows with constant power input*, J. Fluid Mech. 750 (2014), pp. 191–209.
- [11] J.F. Gibson, *Channelflow: A spectral Navier-Stokes simulator in C++*, U. New Hampshire, 2012.
- [12] D. Viswanath, *Recurrent motions within plane Couette turbulence*, J. Fluid Mech. 580 (2007), p. 339.
- [13] H. Dijkstra, F.W. Wubs, A.K. Cliffe, E. Doedel, I.F. Dragomirescu, B. Eckhardt, A.Y. Gelfgat, A.L. Hazel, V. Lucarini, A.G. Salinger, E.T. Phipps, J. Sanchez-Umbria, H. Schuttelaars, L.S. Tuckerman, and U. Thiele, *Numerical Bifurcation Methods and their Application to Fluid Dynamics: Analysis beyond Simulation*, Commun. Comput. Phys. 15 (2014), pp. 1–45.
- [14] W. Heisenberg, *Über die Stabilität und Turbulenz von Flüssigkeitsströmen*, Ann. Phys. 74 (1924).
- [15] C. Lin, *On the stability of two-dimensional parallel flows - Part 2*, Quart. Appl. Math. 3 (1945), pp. 218–234.
- [16] L. Thomas, *The stability of plane Poiseuille flow*, Phys. Rev. 91 (1953), pp. 780–783.
- [17] S.A. Orszag, *Accurate solution of the Orr-Sommerfeld stability equation*, J. Fluid Mech. 50 (1971), pp. 689–703.
- [18] T.S. Chen, and D. Joseph, *Subcritical bifurcation of plane Poiseuille flow*, J. Fluid Mech. 58 (1973), pp. 337–351.
- [19] J.P. Zahn, J. Toomre, E. Spiegel, and D. Gough, *Nonlinear cellular motions in Poiseuille channel flow*, J. Fluid Mech. 64 (1974), pp. 319–345.
- [20] J. Jiménez, *Transition to turbulence in two-dimensional Poiseuille flow*, J. Fluid Mech. 218 (1990), pp. 265–297.

- [21] I. Soibelman, and D.I. Meiron, *Finite-amplitude bifurcations in plane Poiseuille flow: two-dimensional Hopf bifurcation*, J. Fluid Mech. 229 (1991), pp. 389–416.
- [22] D. Grohne *Die Stabilität der ebenen Kanalströmung gegenüber dreidimensionalen Störungen von endlicher Amplitud*, AVA , Gottingen, 1969.
- [23] T. Herbert, *Periodic Secondary Motions In A Plane Channel*, , in *Proc. Fifth Int. Conf. Numer. Methods Fluid Dyn. June 28–July 2, 1976 Twente Univ. Enschede* Springer Berlin / Heidelberg, 1976, pp. 235–240.
- [24] T. Price, M. Brachet, and Y. Pomeau, *Numerical characterization of localized solutions in plane Poiseuille flow*, Phys. Fluids A Fluid Dyn. 5 (1993), p. 762.
- [25] A. Drissi, M. Net, and I. Mercader, *Subharmonic instabilities of Tollmien-Schlichting waves in two-dimensional Poiseuille flow*, Phys. Rev. E 60 (1999), p. 1781.
- [26] F. Mellibovsky, and A. Meseguer, *A mechanism for streamwise localisation of nonlinear waves in shear flows*, J. Fluid Mech. 779 (2015), p. R1.
- [27] P.S. Casas, and À. Jorba, *Hopf bifurcations to quasi-periodic solutions for the two-dimensional plane Poiseuille flow*, Commun. Nonlinear Sci. Numer. Simul. 17 (2012), pp. 2864–2882.
- [28] U. Ehrenstein, and W. Koch, *Three-dimensional wavelike equilibrium states in plane Poiseuille flow*, J. Fluid Mech. 228 (1991), pp. 111–148.
- [29] M. Nagata, and K. Deguchi, *Mirror-symmetric exact coherent states in plane Poiseuille flow*, J. Fluid Mech 735 (2013), p. R4.
- [30] F. Waleffe, *Exact coherent structures in channel flow*, J. Fluid Mech. 435 (2001), pp. 93–102.
- [31] J.F. Gibson, and E. Brand, *Spanwise-localized solutions of planar shear flows*, J. Fluid Mech. 745 (2014), pp. 25–61.
- [32] S. Zammert, and B. Eckhardt, *Periodically bursting edge states in plane Poiseuille flow*, Fluid Dyn. Res. 46 (2014), p. 041419.
- [33] S. Zammert, and B. Eckhardt, *Streamwise and doubly-localised periodic orbits in plane Poiseuille flow*, J. Fluid Mech. 761 (2014), pp. 348–359.
- [34] S. Rawat, C. Cossu, and F. Rincon, *Relative periodic orbits in plane Poiseuille flow*, Comptes Rendus Mécanique 342 (2014), pp. 485–489.
- [35] F. Waleffe, *Homotopy of exact coherent structures in plane shear flows*, Phys. Fluids 15 (2003), p. 1517.
- [36] T.M. Schneider, B. Eckhardt, and J. Yorke, *Turbulence Transition and the Edge of Chaos in Pipe Flow*, Phys. Rev. Lett. 99 (2007), p. 034502.
- [37] R.M. Clever, and F.H. Busse, *Tertiary and quaternary solutions for plane Couette flow*, J. Fluid Mech. 344 (1997), pp. 137–153.
- [38] K. Melnikov, T. Kreilos, and B. Eckhardt, *Long-wavelength instability of coherent structures in plane Couette flow*, Physical Review E 89 (2014), p. 043008.
- [39] M. Pausch, F. Grossmann, B. Eckhardt, and V.G. Romanovski, *Groebner Basis Methods for Stationary Solutions of a Low-Dimensional Model for a Shear Flow*, J. Nonlinear Sci. 24 (2014), pp. 935–948.
- [40] S.I. Chernyshenko, P. Goulart, D. Huang, and A. Papachristodoulou, *Polynomial sum of squares in fluid dynamics: a review with a look ahead*, Philosophical Transactions of the Royal Society of London. Series A 372 (2014), pp. 20130350–20130350.
- [41] D. Huang, S. Chernyshenko, P. Goulart, D. Lasagna, O. Tutty, and F. Fuentes, *Sum-of-squares of polynomials approach to nonlinear stability of fluid flows: an example of application*, Proceedings of the Royal Society A: Mathematical, Physical and Engineering Sciences 471 (2015), p. 20150622.